Particle Growth Behavior of Carbon Supported Pt, Ru, PtRu Catalysts Prepared by an Impregnation Reductive-Pyrolysis Method for Direct Methanol Fuel Cell Anodes

Tomoyuki Kawaguchi, Wataru Sugimoto*, Yasushi Murakami and Yoshio Takasu

Department of Fine Materials Engineering, Faculty of Textile Science and Technology,

Shinshu University

3-15-1 Tokida, Ueda 386-8567, Japan

*Corresponding author. Tel: +81-268-21-5455; Fax: +81-268-22-9048

E-mail: wsugi@shinshu-u.ac.jp

Abstract: Carbon supported Pt, Ru and binary PtRu catalysts were prepared by an impregnation-reductive pyrolysis method at various temperatures using $Pt(NH_3)_2(NO_2)_2$ and $Ru(NO_3)_3$ as precursors. The effect of the reductive pyrolysis temperature on the structure of the metal particles and its relationship to the electrocatalytic activity towards methanol and pre-adsorbed carbon monoxide (CO_{ad}) oxidation was examined. The decomposition temperature of the $Pt_{50}Ru_{50}$ mixed precursor shifted to lower temperature than the Ru single-source precursor. High resolution scanning electron microscopy, X-ray diffraction and CO_{ad} stripping voltammetry of Pt/C and Ru/C indicated that Ru nanoparticles tend to grow drastically when the pyrolysis temperature was increased, while Pt nanoparticles are more resistant to particle growth. Scanning transmission electron microscopy coupled with energy dispersive X-ray spectroscopy analysis showed that a slight compositional variation between individual nanoparticles exists depending on the particle size. The $Pt_{50}Ru_{50}$/C catalyst prepared at 200 ^{o}C exhibited the maximum electrocatalytic activity towards methanol oxidation per mass of PtRu, which was discussed based on the appropriate balance of precursor decomposition and particle growth.

Keywords: Direct methanol fuel cells; Anode catalysts; PtRu; Alloys; Carbon monoxide oxidation; CO stripping voltammetry; Chronoamperometry; STEM-EDX

1. Introduction

Due to the comparatively low operation temperature of the direct methanol fuel cell (DMFC), the poisoning of the anode catalyst by carbon monoxide becomes a major problem. Therefore, the material design of highly active electrocatalysts is an important subject in DMFC development. High-surface area PtRu alloy supported on carbon black is one of the most promising materials as an anode catalyst for DMFC [1-21], because of its high tolerance against carbon monoxide poisoning. The promotion effect of Ru has been mainly discussed based on the so-called “bifunctional mechanism” [4-6, 22-43] or “ligand effect” [37-51] or a mixture of both.

The fundamental properties of the methanol oxidation reaction have been well established using well-defined catalyst, such as Ru decorated single crystals, model electrocatalysts and bulk alloys. In contrast, the understanding of the relationship between the physical and electrocatalytic properties of PtRu nanoparticles supported on carbon black is not as straightforward. The delicate control of composition, particle size, and dispersion state are only a few of the requirements for practical catalysts. The co-impregnation method [13-19, 52-61] is a simple and effective method for the preparation of high surface area carbon supported electrocatalysts. We have shown that the structural properties and electrocatalysis of carbon supported PtRu nanoparticles

vary with the type of precursor employed, and the activity towards methanol electro-oxidation is sensitive to the pyrolysis temperature [14]. In our previous study, we reported the effect of the type of precursor at pyrolysis temperature between 150 and 550 ^{o}C. Reductive pyrolysis at 200^{o}C was preferable for highly active catalysts. For a better understanding of the effect of the pyrolysis temperature on the nanostructure and electrocatalysis of PtRu/C, a systematic study on the nanometer scale is necessary.

Here, we report the particle growth process of Pt, Ru and PtRu catalysts supported on carbon as a function of the pyrolysis temperature up to 800 ^{o}C. Emphasis was placed on the difference in the particle growth behavior of Pt, Ru and PtRu as well as the composition variation between individual PtRu nanoparticles. The activity towards methanol and pre-adsorbed carbon monoxide oxidation of $Pt_{50}Ru_{50}$/C was examined and discussed based on the difference in the structure of the nanoparticles.

2. Experimental

Pt/C, Ru/C and $Pt_{50}Ru_{50}$/C (30 mass% metal) catalysts were prepared by a conventional impregnation method reported previously [14]. The catalysts were prepared by introducing appropriate amounts of carbon black (Vulcan XC-72R) into ethanolic solutions of $Pt(NH_3)_2(NO_2)_2$ (Ishifuku Metal Industry), $Ru(NO_3)_3$ (Tanaka

Kikinzoku Kogyo K. K.), or a 1 : 1 molar ratio of $Pt(NH_3)_2(NO_2)_2$ and $Ru(NO_3)_3$. For the Pt source, 4 mM (M = mol dm^{-3}) $Pt(NH_3)_2(NO_2)_2$ dissolved in ethanol was used. Ethanolic solution of 4 mM $Ru(NO_3)_3$ was used as the Ru source. After thorough mixing, the precursor solution was allowed to dry at 60°C to a powder. The dried powder was then reduced in a tube furnace under flowing H_2(10%)+N_2(90%) gas for 2 h at various temperatures.

The pyrolysis process of the precursor powders was investigated by thermogravimetry (TG, Shimadzu TGA-50) under a constant flow of H_2(10%)+N_2(90%) at a heating rate of 5°C min^{-1}. The structure of Pt/C, Ru/C and $Pt_{50}Ru_{50}$/C was characterized by X-ray diffraction (XRD, Rigaku RINT-2550 with monochromated CuK_α radiation), high-resolution scanning electron microscopy (HRSEM, Hitachi S-5000), high-resolution scanning transmission electron microscopy (HRSTEM, Hitachi HF-2210) and energy dispersive X-ray spectroscopy (EDX, Noran Instruments VOYAGER). Scanning transmission electron microscopy coupled with energy dispersive X-ray spectroscopy (STEM-EDX) analysis was utilized to study the single particle composition of PtRu.

Electrochemical studies were conducted using a three-electrode type beaker cell equipped with a platinum mesh counter electrode, an Ag/AgCl reference electrode, and

the working electrode. A Luggin capillary faced the working electrode at a distance of 2 mm. The working electrodes were prepared by the thin film electrode method [62]. Briefly, 20 mg of the catalyst powder was dispersed in 10 mL of methanol and was subject to ultrasonification for 30 min. Then, 20 μL of the catalyst powder dispersion (40 μg of the catalyst powder containing 12 μg of metal) was dropped on a mirror-polished Glassy Carbon (Tokai Carbon Co., Ltd.) substrate (grade 20SS, 5 mm in diameter). After drying at 60 ^{o}C, 20 μL of a 1 wt% Nafion® alcoholic solution was further dropped on the electrode surface to stabilize the electrocatalysts to the Glassy Carbon rod surface. All potentials throughout the present paper are given in the reversible hydrogen electrode (RHE) scale. The electrocatalytic oxidation of pre-adsorbed carbon monoxide (CO_{ad}) was measured by CO_{ad} stripping voltammetry at a scan rate of 10 mV s^{-1}. CO gas was purged into the cell (0.5 M H_2SO_4, 60 ^{o}C) for 40 min to allow adsorption of CO onto the accessible metal surface while maintaining a constant voltage of 270 mV vs. RHE. Excess CO was purged out with N_2 gas for 40 min. The amount of CO_{ad} was evaluated by integration of the CO_{ad} stripping peak, corrected for the electrical double-layer capacitance. The electrochemical oxidation of methanol was characterized by the quasi steady-state current density at 470 mV vs. RHE in 1.0 M CH_3OH + 0.5 M H_2SO_4 solution. All electrochemical measurements were carried out at

60 ^{o}C.

3. Results and discussion

3.1. Carbon supported platinum

The pyrolysis process in H_2(10%)+N_2(90%) for the Pt/C precursor powder is shown in Fig. 1a. The decomposition of the Pt/C precursor was completed at about 170^{o}C. HRSEM images of Pt/C pyrolyzed at various temperatures are shown in Fig. 2. The histograms of the particle size estimated from 100 particles as a function of the pyrolysis temperature are shown in Fig. 3. More than 80% of the Pt particles were in the range of 2-5 nm, irrespective of the pyrolysis temperature. The relative abundance of small particles (< 3 nm) decreased with increasing pyrolysis temperatures (200^{o}C; 28%, 450^{o}C; 12%, 800^{o}C; 8%), while that of particles in the range of 3 ~ 4 nm slightly increased with increasing pyrolysis temperature (200^{o}C; 33%, 450^{o}C; 45%, 800^{o}C; 50%). The relative abundance of larger particles (**>** 4 nm) was not significantly affected by the pyrolysis temperature (200^{o}C; 39%, 450^{o}C; 43%, 800^{o}C; 42%). The XRD patterns of Pt/C pyrolyzed at various temperatures are shown in Fig. 4. The XRD patterns could be indexed based on the fcc structure of Pt metal. The sharpening of the XRD peaks indicates an increase in the average crystallite size with increasing

temperature of pyrolysis.

----- Fig. 1 -----

----- Fig. 2 -----

----- Fig. 3 -----

----- Fig. 4 -----

The CO_{ad} stripping voltamograms of Pt/C are shown in Fig. 5. The peak-top of the CO_{ad} oxidation appeared at 670 mV vs. RHE. The mean particle size of Pt calculated from the electrochemically active surface area increased slightly with increasing pyrolysis temperature; 2.5, 2.9 and 3.4 nm for the products pyrolyzed at 200, 450 and 800^{o}C, respectively. This observation is consistent with the sharpening of the XRD peak suggesting an increase is crystallite size, which is particularly notable for the 800 ^{o}C-pyrolyzed product.

----- Fig. 5 -----

3.2. Carbon supported ruthenium

The decomposition of the Ru/C precursor powder was completed at about 250^{o}C (Fig. 1b), which is 80 ^{o}C higher than the Pt/C precursor (Fig. 1a). HRSEM images of Ru/C pyrolyzed at various temperatures are shown in Fig. 6. The particle size distribution at different pyrolysis temperature is shown in Fig. 7. In contrast to Pt/C, Ru particles

clearly showed a tendency to grow with increasing temperature of pyrolysis. The relative abundance of particles larger than 4 nm significantly increased with increasing pyrolysis temperature (200 ^{o}C; 7%, 450 ^{o}C; 39%, 800 ^{o}C; 62%). As shown in Fig. 6c, Ru particles as large as 30 nm (marked with arrows) were also observed besides the smaller particles (2 nm) for the Ru/C catalyst prepared at 800 ^{o}C.

----- Fig. 6 -----

----- Fig. 7 -----

The XRD patterns of Ru/C pyrolyzed at various temperatures are shown in Fig. 8. The XRD patterns could be indexed based on the hcp structure of Ru metal. The sharpening of the XRD peaks indicates an increase in the average crystallite size with increasing temperature of pyrolysis. The sharpening of the peaks was more apparent for Ru/C compared to Pt/C, consistent with the HR-SEM analysis revealing an increase in particle size.

----- Fig. 8 -----

The CO_{ad} stripping voltamograms of Ru/C pyrolyzed at various temperatures are shown in Fig. 9. The peak-top of the CO_{ad} oxidation appeared at 450-480 mV vs. RHE on Ru/C. The CO_{ad} oxidation charge decreased drastically with increasing pyrolysis temperature. The quantitative evaluation of the electrochemically active surface from

CO_{ad} stripping voltammetry for Ru/C is complicated [21] and is strongly dependent on the measuring conditions such as pre-adsorption potential and operating temperature. Here, we have not optimized the pre-adsorption potential, thus only a quantitative assessment can be discussed, and the discussion on the CO_{ad} oxidation on Ru/C will be confined to the relative change in the amount of adsorbed CO. The CO_{ad} oxidation charge for Ru/C pyrolyzed at 800 ^{o}C was only 21% of the value for Ru/C pyrolyzed at 200 ^{o}C. The decrease in the electrochemically active surface area with increasing pyrolysis temperature for Ru/C was much more profound compared to Pt/C. These results are consistent with the particle size analysis of Pt/C and Ru/C by HR-SEM and XRD. The particle growth behavior of the Ru particles is more significant than the Pt particles. The difference in the particle growth behavior of Pt and Ru particles is probably due to differences in the physical properties between Pt and Ru (for example, interaction with hydrogen, surface free energy and interaction with the carbon support, *etc*.).

----- Fig. 9 -----

3.3. Carbon supported $Pt_{50}Ru_{50}$

The decomposition of the binary $Pt_{50}Ru_{50}$/C precursor was completed at 200^{o}C (Fig. 1c). In the case of the PtRu mixed precursor, the Pt precursor and the Ru precursor

decomposed simultaneously in a single process. The decomposition temperature of the PtRu mixed precursor was lower than that of the Ru-single source precursor (Fig. 1b). These facts suggest that the Pt and Ru sources were mixed at an atomic level in the precursor solution. The single step decomposition process of the PtRu mixed precursor is preferable from the standpoint of bi-metal alloying, since nucleation of both metals will occur simultaneously.

Figure 10 shows the XRD patterns of $Pt_{50}Ru_{50}$/C pyrolyzed at various temperatures. The XRD peak sharpened with increasing pyrolysis temperature especially above 600 ^{o}C, suggesting an increase in the particle size and/or an increase in crystallinity. With increasing pyrolysis temperature from 150 to 450 ^{o}C, the fcc(220) peak shifted to higher reflection angles suggesting that more amounts of Ru were introduced into the fcc structure.

----- Fig. 10 -----

The STEM images of $Pt_{50}Ru_{50}$/C prepared at 200, 450, and 800 ^{o}C are shown in Fig. 11. The average bulk Ru content obtained by EDX analysis was in accordance with the nominal contents Pt:Ru = 45:55, 51:49, 48:52 Ru mol% at 200, 450 and 800 ^{o}C, respectively. The Ru content of individual particles with different particle size is shown in Fig. 12 along with the relative abundance as a function of the pyrolysis temperature.

Approximately 70-80% of the measured particles were in the range of 2-5 nm for the catalysts, irrespective of the pyrolysis temperature. The majority of the alloy particles (80% or more) in the $Pt_{50}Ru_{50}$/C catalysts prepared at 200 to 450 ^{o}C is in the range of 2-5 nm, in accordance with our previous results [14]. The Ru contents for these individual particles were close to unity. For particles less than 2 nm or more than 5 nm in diameter (about 20-30% of all measured particles), the Ru content tended to deviate from the nominal content. The histogram also shows that the relative abundance of relatively large particles (>5 nm) increased with increasing pyrolysis temperatures (200^{o}C; 3%, 450^{o}C; 20%, 800^{o}C; 26%), which is consistent with the XRD results. In particular, PtRu particles larger than 30 nm were observed when the pyrolysis temperature was 800 ^{o}C (Fig. 11c), indicating that the high-temperature particle growth behavior of PtRu particles is similar to that of Ru particles. That is, PtRu particles tend to sinter at high temperature.

----- Fig. 11 -----

----- Fig. 12 -----

The CO_{ad} stripping voltamograms $Pt_{50}Ru_{50}$/C pyrolyzed at various temperatures are shown in Fig. 13. The peak-top of the CO_{ad} oxidation appeared at 450-465 mV vs. RHE. Similar to the behavior of Ru/C and Pt/C, the CO_{ad} oxidation charge decreased for

$Pt_{50}Ru_{50}$/C with increasing pyrolysis temperatures. In addition, an oxidation shoulder peak is observed near 600 mV vs. RHE. These peaks are attributed to the CO_{ad} oxidation on Pt or Pt-rich surfaces since the electrode potentials are close to that of Pt/C (see Fig. 5) [19].

----- Fig. 13 -----

The effect of the pyrolysis temperature on the electrocatalytic activity for methanol oxidation is shown in Fig. 14. The sample pyrolyzed at 200 ^{o}C exhibited the highest current density with 42 A g^{-1}_{PtRu}. Although the alloying of ruthenium with platinum progresses as the pyrolysis temperature is increased, large particles are also generated with increasing pyrolysis temperature. Such features reduce the mass activity for methanol oxidation. In addition, if surface Pt-rich particles exist, these may also contributed to the decrease in activity [7]. The low activity of the catalyst pyrolyzed at 150 ^{o}C is most likely due to the incomplete decomposition of the PtRu precursor (Fig. 1 c). The decomposition of the PtRu precursor occurs in the range of 150 ^{o}C to 200 ^{o}C. If the precursor is not completely reduced to the metal state, residual organics should hinder the electrocatalytic activity. This can be seen in the cyclic voltamograms (Fig. 13), which show that the electrocatalyst pyrolyzed at 150 ^{o}C tends to have a smaller electric double-layer capacitance. This is suggestive of a low electrochemically active

surface area owing to the residual species covering the electrocatalyst surface. The catalyst preparation should preferably be around 200 ^{o}C where sintering is inhibited and good dispersion state as well as good alloying state of the $Pt_{50}Ru_{50}$ nanoparticles are achieved.

----- Fig. 14 -----

Particle growth phenomenon is one of the causes of catalyst activity degradation in an operating fuel cell. There may be some similarities between the high-temperature particle growth process observed in this study and the catalyst activity degradation process in a practical fuel cell. The present results of the particle growth behavior of PtRu particles at high temperature may give insights into the catalyst degradation process in actual fuel cells.

4. Conclusions

The structures of Pt, Ru and $Pt_{50}Ru_{50}$ nanoparticles supported on carbon and its relationship to the electro-catalytic activity towards CO_{ad} and methanol oxidation was examined. HRSEM analysis, XRD and CO_{ad} stripping voltammetry showed that the particle size drastically increased with the increase in the pyrolysis temperature for Ru/C catalyst, in contrast to Pt/C. Analysis of the size and composition of individual $Pt_{50}Ru_{50}$ nanoparticles by STEM-EDX showed that 70-80% of the nanoparticles had a

size of 2-5 nm and composition close to unity. The highest mass activity of the $Pt_{50}Ru_{50}$/C prepared at 200 ^{o}C was suggested to be a result of the suitable balance between the sintering state, dispersion state and alloying state.

Acknowledgements

The authors are grateful to Ishifuku Metal Industry Co. for kindly supplying $Pt(NH_3)_2(NO_2)_2$. This work was supported in part by a Polymer Electrolyte Fuel Cell Program from the New Energy and Industrial Technology Development Organization (NEDO) of Japan, in collaboration with Toray Industries, Inc, and a MEXT 21st Century COE Program of Japan.

References

[1] M. Hogarth, T. Ralph, Platinum Met. Rev. 46 (2002) 146.

[2] A. S. Aricò, Srinivasan, V. Antonucci, Fuel Cells 1 (2001) 1.

[3] J. O'M. Bockris, H. Wroblowa, J. Electroanal. Chem. 7 (1964) 428.

[4] M. Watanabe, S. Motoo, J. Electroanal. Chem. 60 (1975) 267.

[5] M. Watanabe, S. Motoo, J. Electroanal. Chem. 60 (1975) 275.

[6] H. N. Dinh, X. Ren, F. H. Garzon, P. Zelenay, S. Gottesfeld, J. Electroanal. Chem. 491 (2000) 222.

[7] B. D. McNicol, R. T. Short, J. Electroanal. Chem. 81 (1977) 249.

[8] J. B. Goodenough, A. Hamnett, B. J. Kennedy, R. Manoharan, S. A. Weeks, J. Electroanal. Chem. 240 (1988) 133.

[9] A. Hamnett, S. A. Weeks, B. J. Kennedy, G. Troughton, P. A. Christensen, Ber. Bunsen-Ges. 94 (1990) 1014.

[10] A. S. Aricò, P. Creti, H. Kim, R. Mantegna, N. Giordano, V. Antonucci, J. Electrochem. Soc. 143 (1996) 3950.

[11] A. S. Aricò, A. K. Shukla, K. M. El-Khatib, P. Creti, V. Antonucci, J. Appl. Electrochem. 29 (1999) 671.

[12] T. J. Schmidt, H. A. Gasteiger, R. J. Behm, Electrochem. Commum. 1 (1999) 1.

[13] A. S. Aricò, P. Creti, E. Modica, G. Monforte, V. Baglio, V. Antonucci, Electrochim. Acta 45 (2000) 4319.

[14] Y. Takasu, T. Fujiwara, Y. Murakami, K. Sasaki, M. Oguri, T. Asaki, W. Sugimoto, J. Electrochem. Soc. 147 (2000) 4421.

[15] Y. Takasu, H. Itaya, T. Iwazaki, R. Miyoshi, T. Ohnuma, W. Sugimoto, Y. Murakami, Chem. Commun. 2001 (2001) 341.

[16] Y. Takasu, T. Kawaguchi, W. Sugimoto, Y. Murakami, Electrochim. Acta 48 (2003) 3861.

[17] Y. Takasu, W. Sugimoto, Y. Murakami, Catal. Surv. Asia 7 (2003) 21.

[18] Y. Takasu, H. Itaya, T. Kawaguchi, W. Sugimoto, Y. Murakami, Stud. Surf. Sci. Catal. 145 (2003) 279.

[19] T. Kawaguchi, W. Sugimoto, Y. Murakami, Y. Takasu, Electrochem. Commun. 6 (2004) 480.

[20] A. V. Tripkovíc, K. D. Popovíc, B. N. Grgur, B. Blizanac, P. N. Ross, N. M. Markovic, Electrochim. Acta 47 (2002) 3707.

[21] C. Roth, N. Martz, F. Hahn, J.-M. Léger, C. Lamy, H. Fuess, J. Electrochem. Soc. 149 (2002) E433.

[22] T. Yajima, H. Uchida, M. Watanabe, J. Phys. Chem. B 108 (2004) 2654.

[23] M. Watanabe, S. Motoo, Denki Kagaku (presently Electrochemistry) 41 (1973) 190.

[24] T. Yajima, H. Uchida, M. Watanabe, J. Phys. Chem. B 108 (2004) 2654.

[25] E. Ticanelli, J. G. Beery, M. T. Paffett, S. Gottesfeld, J. Electroanal. Chem. 258 (1989) 61.

[26] X. Ren, P. Zelenay, S. Thomas, J. Davey, S. Gottesfeld, J. Power Sources 86 (2000) 111.

[27] H. A. Gasteiger, N. Markovic, P. N. Ross Jr., E. J. Cairns, J. Phys. Chem. 98 (1994) 617.

[28] H. A. Gasteiger, N. Markovic, P. N. Ross Jr., E. J. Cairns, J. Electrochem. Soc. 141 (1994) 1795.

[29] H. A. Gasteiger, N. Markovic, P. N. Ross Jr., E. J. Cairns, Electrochim. Acta 39 (1994) 1825.

[30] H. A. Gasteiger, N. M. Markovic, P. N. Ross Jr., J. Phys. Chem. 99 (1995) 8290.

[31] H. A. Gasteiger, N. M. Markovic, P. N. Ross Jr. J., Phys. Chem. 99 (1995) 16757.

[32] S. Swathirajan, Y. M. Mikhail, J. Electrochem. Soc. 138 (1991) 1321.

[33] J. Munk, P. A. Christensen, A. Hamnett, E. Skou, J. Electroanal. Chem. 401 (1996) 215.

[34] H. Wang, C. Wingender, H. Baltruschat, M. Lopez, M. T. Reetz, J. Electroanal. Chem. 509 (2001) 163.

[35] L. Giorgi, A. Pozio, C. Bracchini, R. Giorgi, S. Turtu, J. Appl. Electrochem. 31 (2001) 325.

[36] A. S. Aricò, P. L. Antonucci, E. Modica, V. Baglio, H. Kim, V. Antonucci, Electrochim. Acta 47 (2002) 3237.

[37] H. A. Gasteiger, N. Markovic, P. N. Ross Jr., E. J. Cairns, J. Phys. Chem. 97 (1993) 12020.

[38] G. Tremiliosi-Filho, H. Kim, W. Chrzanowski, A. Wieckowski, B. Grzybowska, P. Kulesza, J. Electroanal. Chem. 467 (1999)143.

[39] P. Waszczuk, A. Wieckowski, P. Zelenay, S. Gottesfeld, C. Coutanceau, J.-M. Léger, C. Lamy, J. Electroanal. Chem. 511 (2001) 55.

[40] P. Waszczuk, G.-Q. Lu, A. Wieckowski, C. Lu, C. Rice, R. I. Masel, Electrochim. Acta 47 (2002) 3637.

[41] J. C. Davies, B. E. Hayden, D. J. Pegg, Surf. Sci. 467 (2000) 118.

[42] M. Watanabe, Y. M. Zhu, H. Uchida, Electrochemistry 68 (2000) 244.

[43] H. Igarashi, T. Fujino, Y. Zhu, H. Uchida, M. Watanabe, Phys. Chem. Chem. Phys. 3 (2001) 306.

[44] T. Iwasita, F. C. Nart, W. Vielstich, Ber. Bunsen-Ges. 94 (1990) 1030.

[45] M. Krausa, W. Vielstich, J. Electroanal. Chem. 379 (1994) 307.

[46] W. F. Lin, M. S. Zei, M. Eiswirth, G. Ertl, T. Iwasita, W. Vielstich, J. Phys. Chem. B 103 (1999) 6968.

[47] R. Liu, H. Iddir, Q. Fan, G. Hou, A. Bo, K. L. Ley, E. S. Smotkin, Y.-E. Sung, H. Kim, S. Thomas, A. Wieckowski, J. Phys. Chem. B 104 (2000) 3518.

[48] C. Lu, C. Rice, R. I. Masel, P. K. Babu, P. Waszczuk, H. S. Kim, E. Oldfield, A. Wieckowski, J. Phys. Chem. B 106 (2002) 9581.

[49] T. Frelink, W. Visscher, J. A. R. van Veen, Surf. Sci. 335 (1995) 353.

[50] T. Frelink, W. Visscher, J. A. R. van Veen, Langmuir 12 (1996) 3702.

[51] M. M. P. Janssen, J. Moolhuysen, Electrochim. Acta 21 (1976) 869.

[52] E. S. Steigerwalt, G. A. Deluga, C. M. Lukehart, J. Phys. Chem. B 106 (2002) 760.

[53] E. S. Steigerwalt, G. A. Deluga, D. E. Cliffel, C. M. Lukehart, J. Phys. Chem. B 105 (2001) 8097.

[54] G. Che, B. B. Lakshmi, C. R. Martin, E. R. Fisher, Langmuir 15 (1999) 750.

[55] G. Che, B. B. Lakshmi, E. R. Fisher, C. R. Martin, Nature 393 (1998) 346.

[56] N. Fujiwara, K. Yasuda, T. Ioroi, Z. Siroma, Y. Miyazaki, Electrochim. Acta 70 (2002) 988.

[57] C. W. Hills, M. S. Nashner, A. I. Frenkel, J. R. Shapley, R. G. Nuzzo, Langmuir 15 (1999) 690.

[58] M. S. Nashner, A. I. Frenkel, D. Somerville, C. W. Hills, J. R. Shapley, R. G. Nuzzo, J. Am. Chem. Soc. 120 (1998) 8093.

[59] M. S. Nashner, A. I. Frenkel, D. L. Adler, J. R. Shapley, R. G. Nuzzo, J. Am. Chem. Soc. 119 (1997) 7760.

[60] C. W. Hills, N. H. Mack, R. G. Nuzzo, J. Phys. Chem. B 107 (2003) 2626.

[61] E. Antolini, F. Cardellini, J. Alloys Compd. 315 (2001) 118.

[62] T. J. Schmidt, H. A. Gasteiger, G. D. Stäb, P. M. Urban, Kolb, D. M. Kolb, R. J. Behm, J. Electrochem. Soc. 145 (1998) 2354.

[63] D. Chu, S. Gilman, J. Electrochem. Soc. 143 (1996) 1685.

[64] H. A. Gasteiger, P. N. Ross, E. J. Cairns, Surf. Sci. 293 (1993) 67.

[65] E. Antolini, L. Giorgi, F. Cardellini, E. Passalacqua,. J. Solid State Electrochem. 5 (2001) 131.

[66] V. Radmilovic, H. A. Gasteiger, P. N. Ross Jr., J. Catal. 154 (1995) 98.

[67] C. He, H. R. Kunz, J. M. Fenton, J. Electrochem. Soc. 144 (1997) 970.

[68] E. Antolini, Mater. Chem. Phys. 78 (2003) 563.

FIGURE LEGENDS

Fig. 1. The TG curves of a) $Pt(NH_3)_2(NO_2)_2$, b) $Ru(NO_3)_3$ and c) $Pt(NH_3)_2(NO_2)_2$+ $Ru(NO_3)_3$ supported on Vulcan XC-72R carbon black powder under flowing H_2(10%)-N_2(90%).

Fig. 2. HR-SEM images of Pt/C pyrolyzed under reducing condition at a) 200, b) 450 and c) 800 ^oC.

Fig. 3. Histograms of Pt/C pyrolyzed under reducing condition at a) 200, b) 450 and c) 800 ^oC.

Fig. 4. The XRD patterns of Pt/C pyrolyzed under reducing condition at a) 200, b) 450 and c) 800 ^oC.

Fig. 5. The CO_{ad}-stripping voltamograms at 10 mV s^{-1} of Pt/C pyrolyzed at a) 200, b) 450 and c) 800 ^oC in 0.5 M H_2SO_4 (60 ^oC).

Fig. 6. HR-SEM images of Ru/C pyrolyzed under reducing condition at a) 200, b) 450 and c) 800 ^oC.

Fig. 7. Histograms of Ru/C pyrolyzed under reducing condition at a) 200, b) 450 and c) 800 ^oC.

Fig. 8. The XRD patterns of Ru/C pyrolyzed under reducing condition at a) 200, b) 450 and c) 800 ^oC.

Fig. 9. The CO_{ad}-stripping voltamograms at 10 mV s^{-1} of Ru/C pyrolyzed at a) 200, b) 450 and c) 800 ^{o}C in 0.5 M H_2SO_4 (60 ^{o}C).

Fig. 10. The XRD patterns of $Pt_{50}Ru_{50}$/C catalysts prepared at a) 150, b) 200, c) 300, d) 450, e) 500, f) 600 and g) 800 ^{o}C.

Fig. 11. The STEM images of $Pt_{50}Ru_{50}$/C catalysts pyrolyzed at a) 200, b) 450 and c) 800 ^{o}C.

Fig. 12. The Ru contents of individual particles in $Pt_{50}Ru_{50}$/C pyrolyzed under reducing condition at a) 200, b) 450 and c) 800 ^{o}C (left axis) and the relative abundance as a function of the particle size (right axis) estimated from STEM-EDX analysis.

Fig. 13. The CO_{ad}-stripping voltamograms at 10 mV s^{-1} of $Pt_{50}Ru_{50}$/C catalysts pyrolyzed at a) 150, b) 200, c) 450 and d) 800 ^{o}C in 0.5 M H_2SO_4 (60 ^{o}C).

Fig. 14. The methanol oxidation current density as a function of measurement time for $Pt_{50}Ru_{50}$/C catalysts pyrolyzed at a) 150, b) 200, c) 450 and d) 800 ^{o}C in 0.5 M H_2SO_4 + 1 M CH_3OH at 60 ^{o}C at 470 mV vs. RHE.

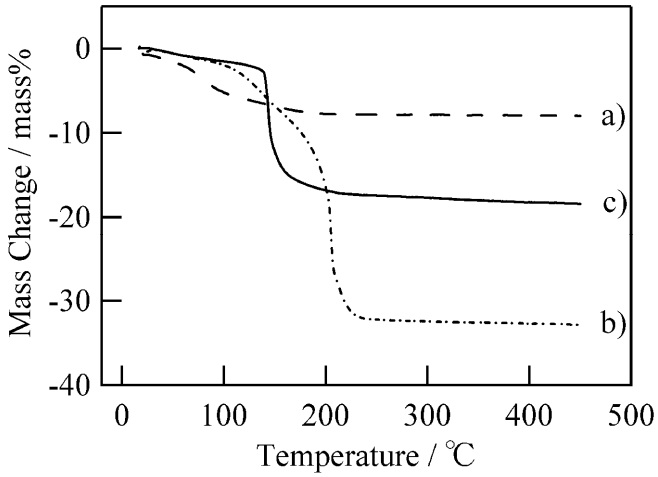
Mass Change / mass%
0
-10
-20
-30
-40
0
100
200
300
400
500
Temperature / ℃
a)
c)
b)

Figure 1

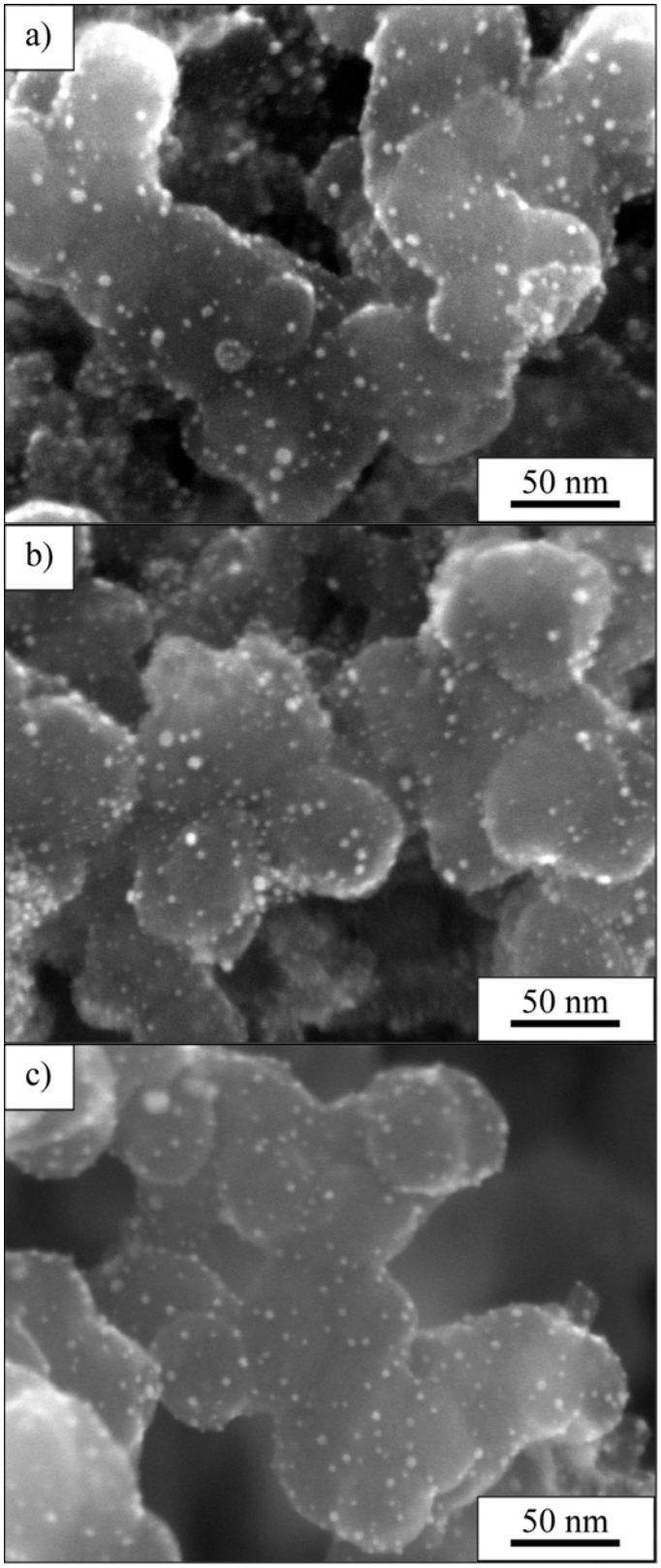

Figure 2

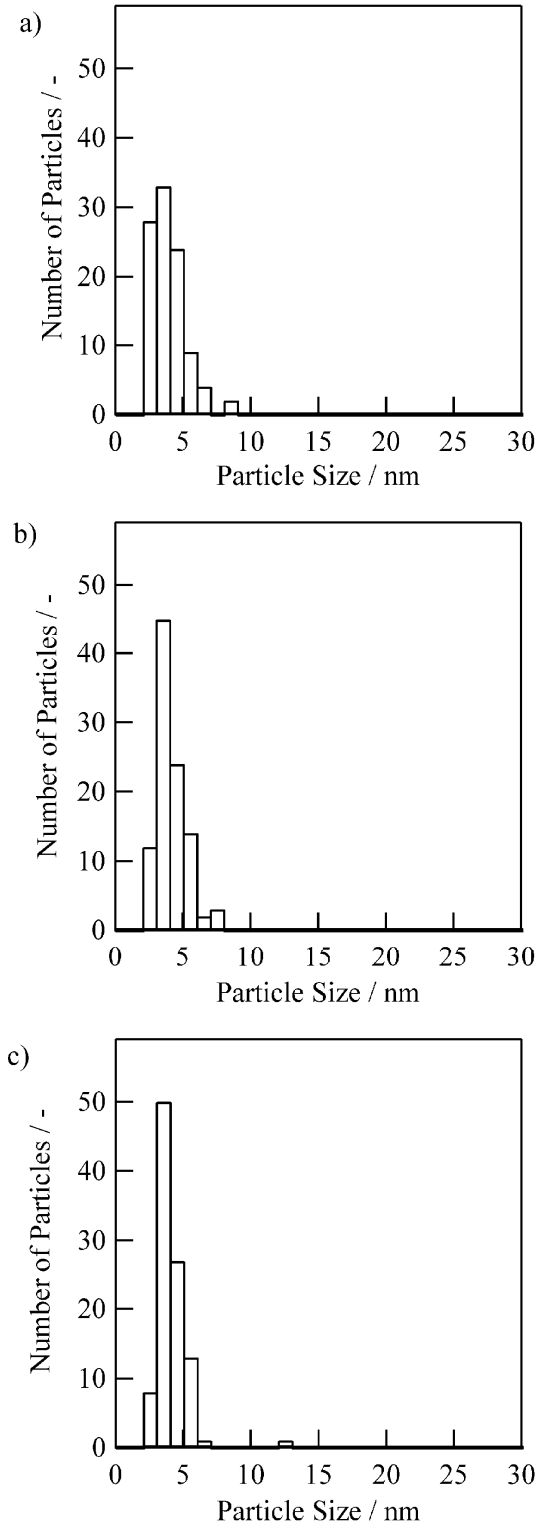
a)
Number of Particles / -
0
10
20
30
40
50
0
5
10
15
20
25
30
Particle Size / nm
b)
Number of Particles / -
0
10
20
30
40
50
0
5
10
15
20
25
30
Particle Size / nm
c)
Number of Particles / -
0
10
20
30
40
50
0
5
10
15
20
25
30
Particle Size / nm

Figure 3

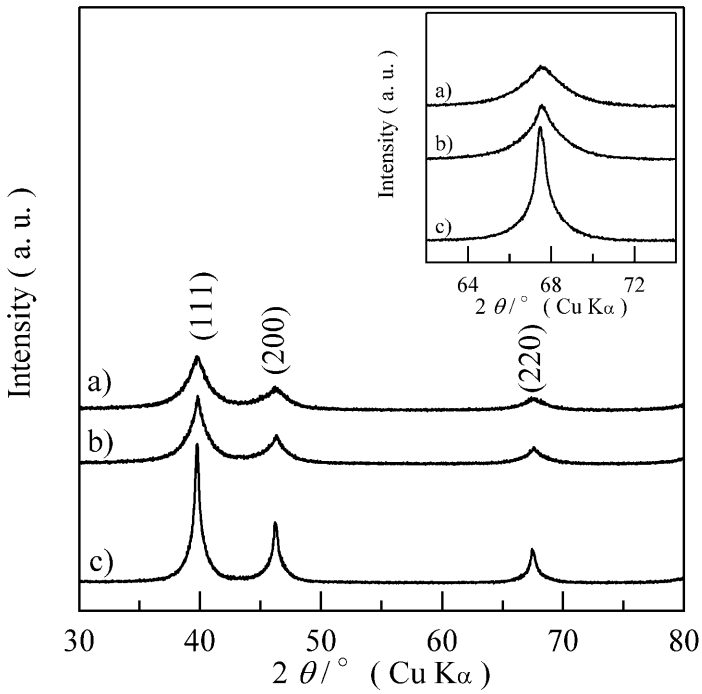
Intensity (a. u.)
(111)
(200)
(220)
a)
b)
c)
30
40
50
60
70
80
2 θ/° (Cu Kα)
Intensity (a. u.)
a)
b)
c)
64
68
72
2 θ/° (Cu Kα)

Figure 4

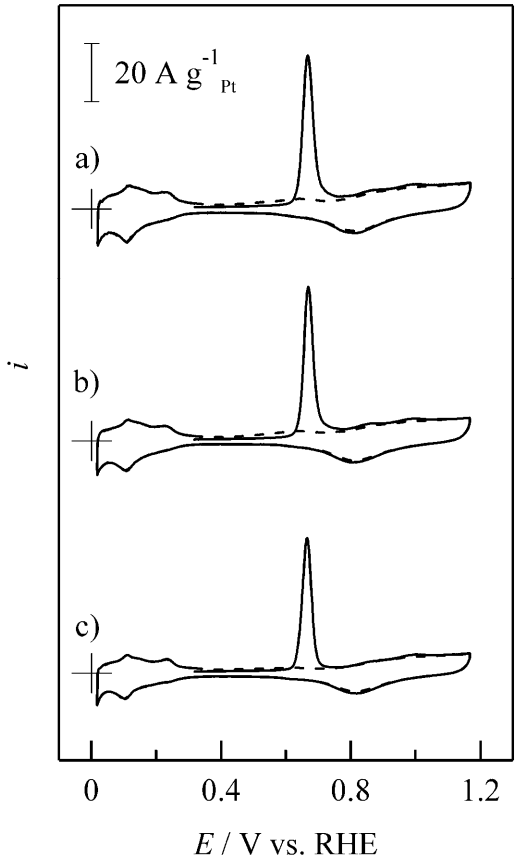

Figure 5

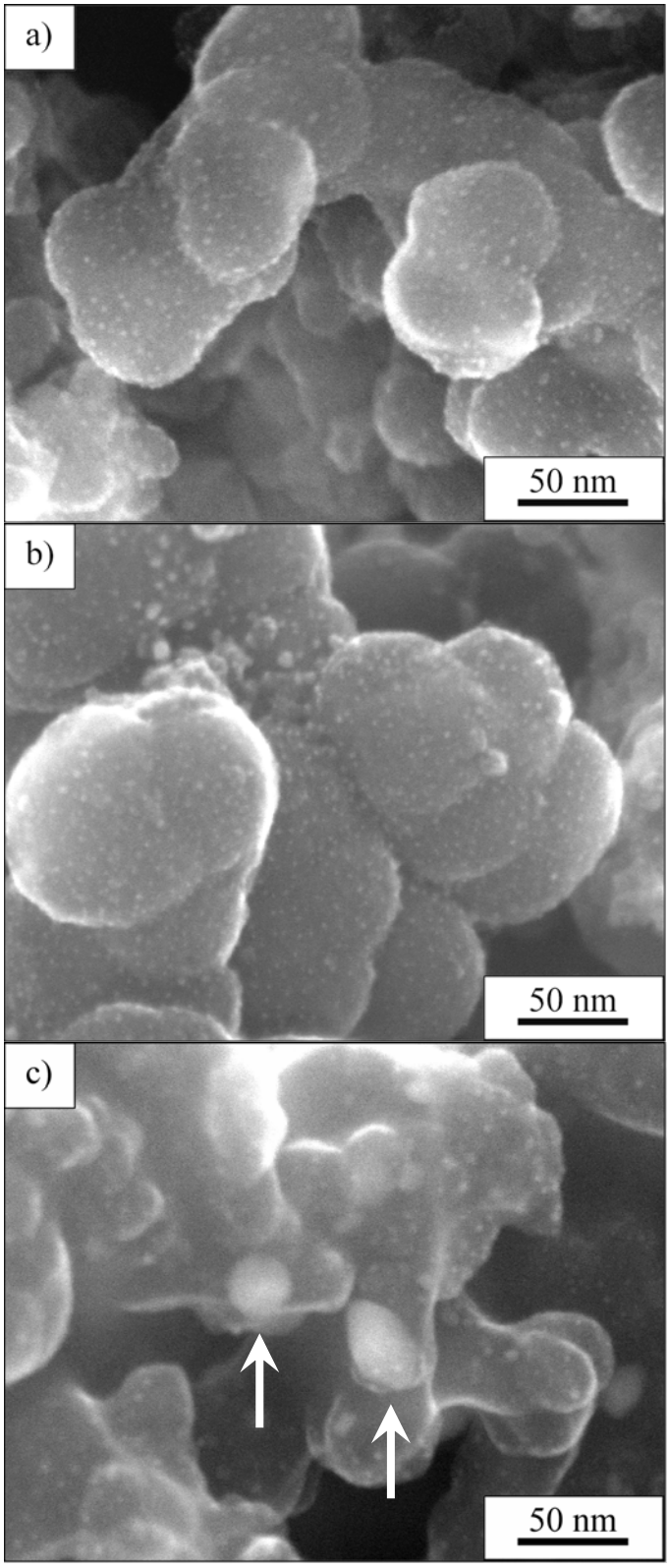

Figure 6

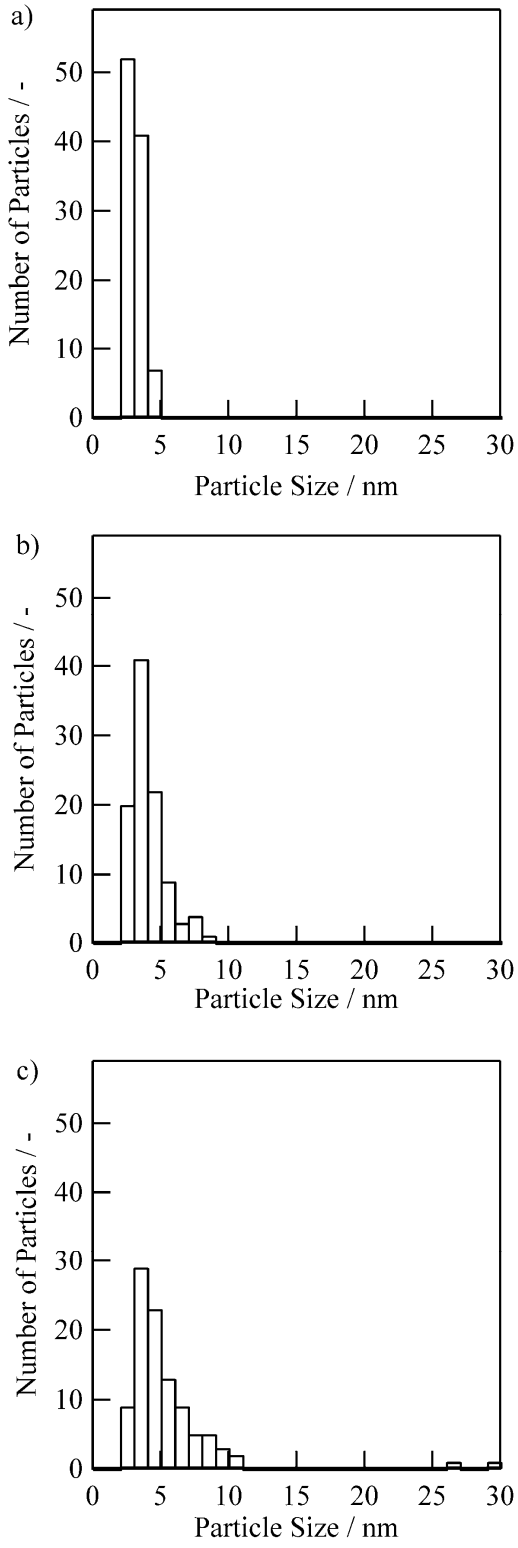
a)
Number of Particles / -
0
10
20
30
40
50
0
5
10
15
20
25
30
Particle Size / nm
b)
Number of Particles / -
0
10
20
30
40
50
0
5
10
15
20
25
30
Particle Size / nm
c)
Number of Particles / -
0
10
20
30
40
50
0
5
10
15
20
25
30
Particle Size / nm

Figure 7

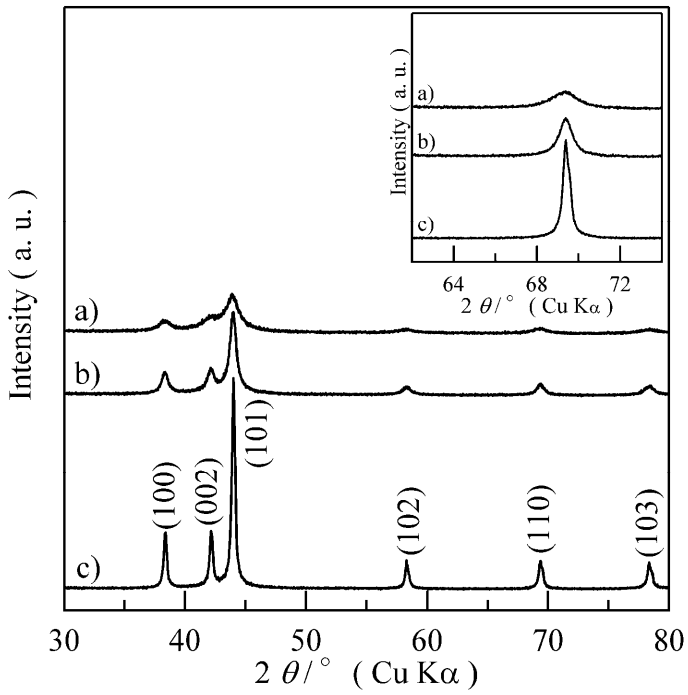
Intensity (a. u.)
a)
b)
c)
(100)
(002)
(101)
(102)
(110)
(103)
30
40
50
60
70
80
2 θ / ° (Cu Kα)
Intensity (a. u.)
a)
b)
c)
64
68
72
2 θ / ° (Cu Kα)

Figure 8

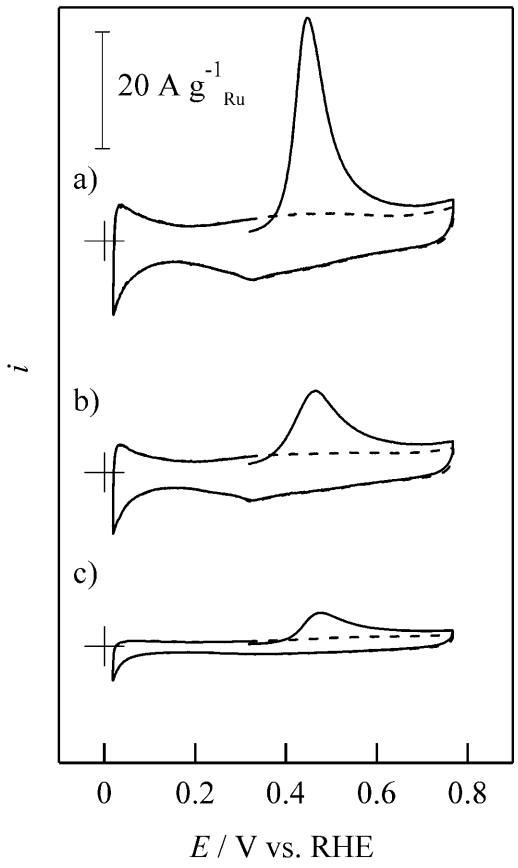

Figure 9

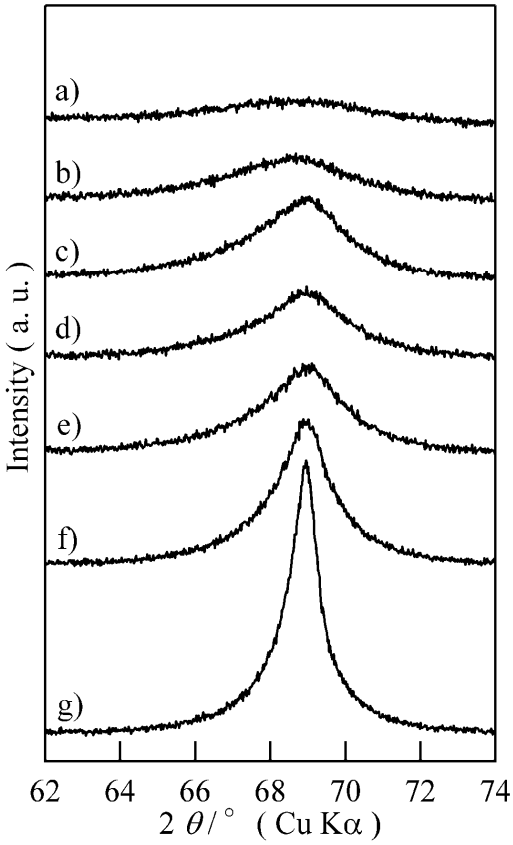

Figure 10

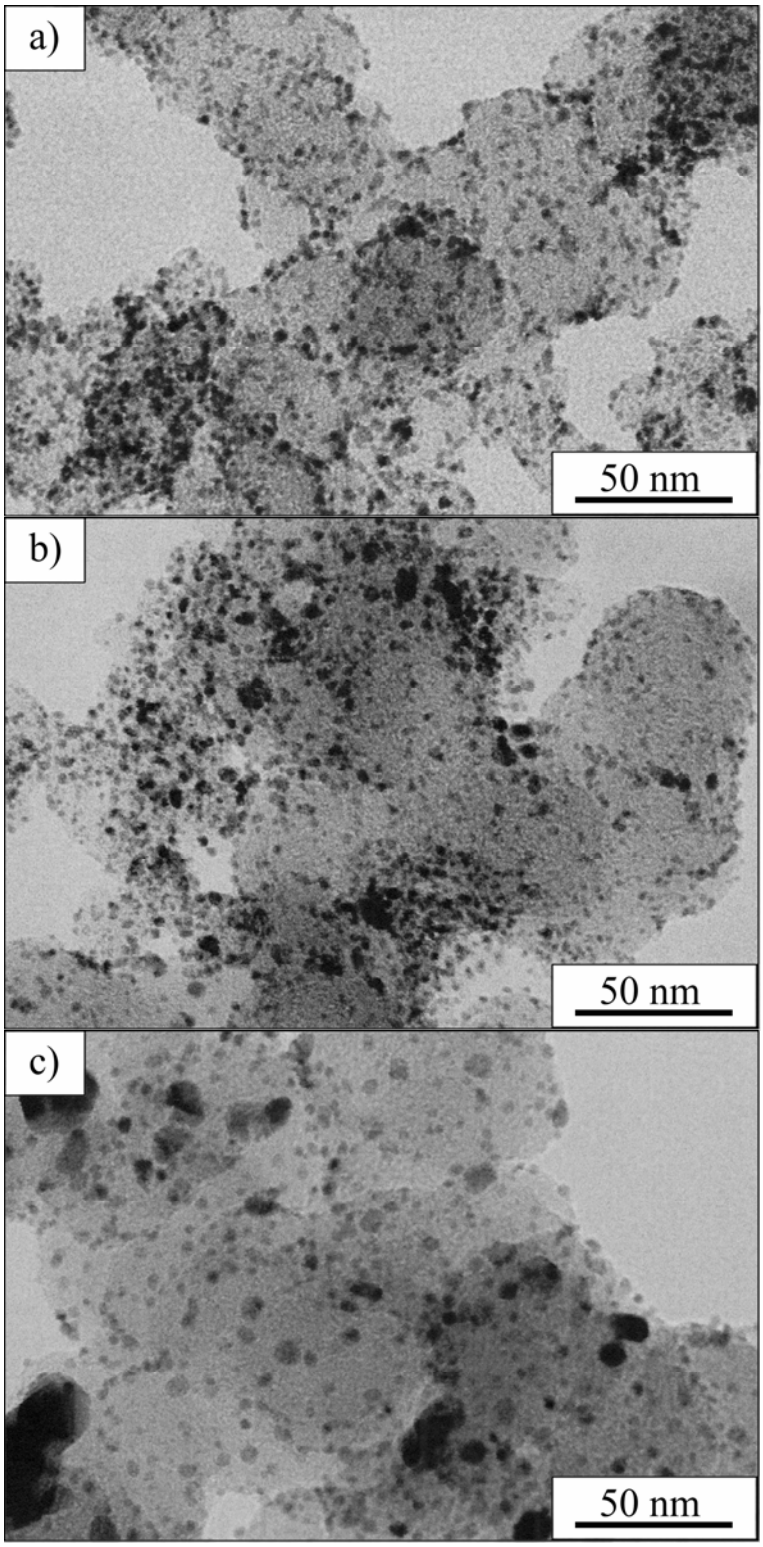

Figure 11

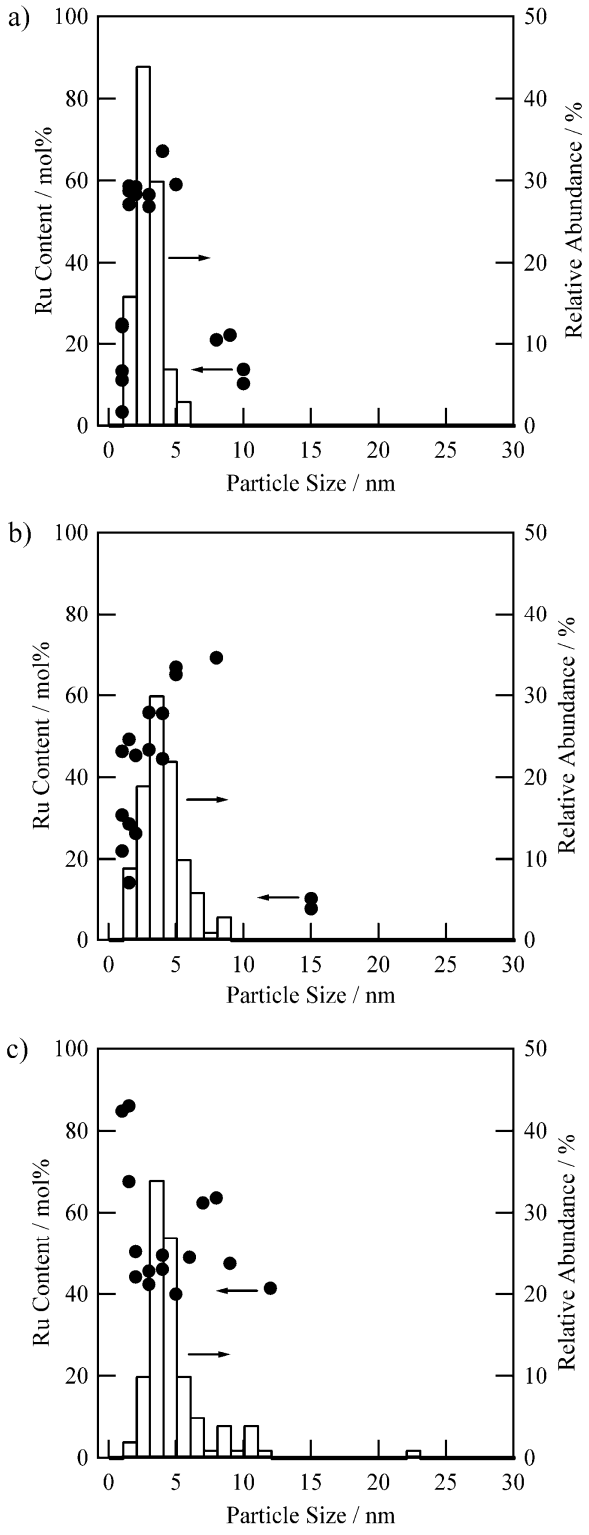
a)
b)
c)
Ru Content / mol%
Relative Abundance / %
Particle Size / nm
0
5
10
15
20
25
30
0
20
40
60
80
100
0
10
20
30
40
50

Figure 12

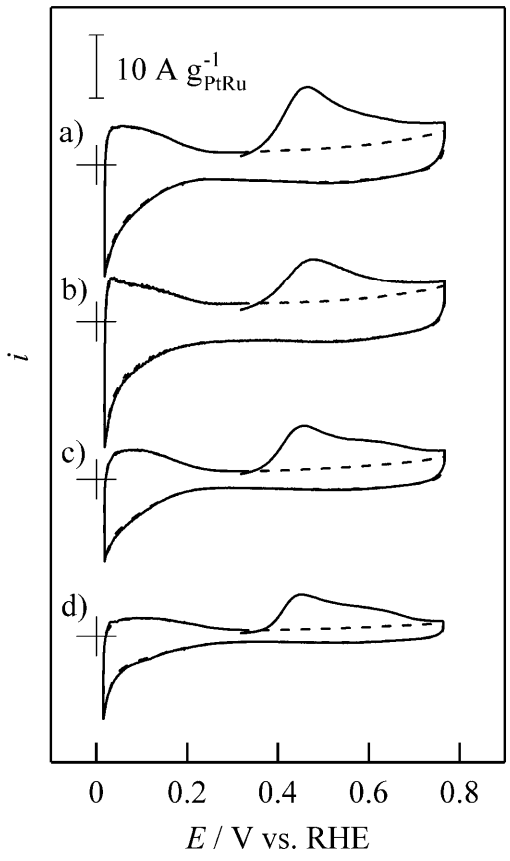

Figure 13

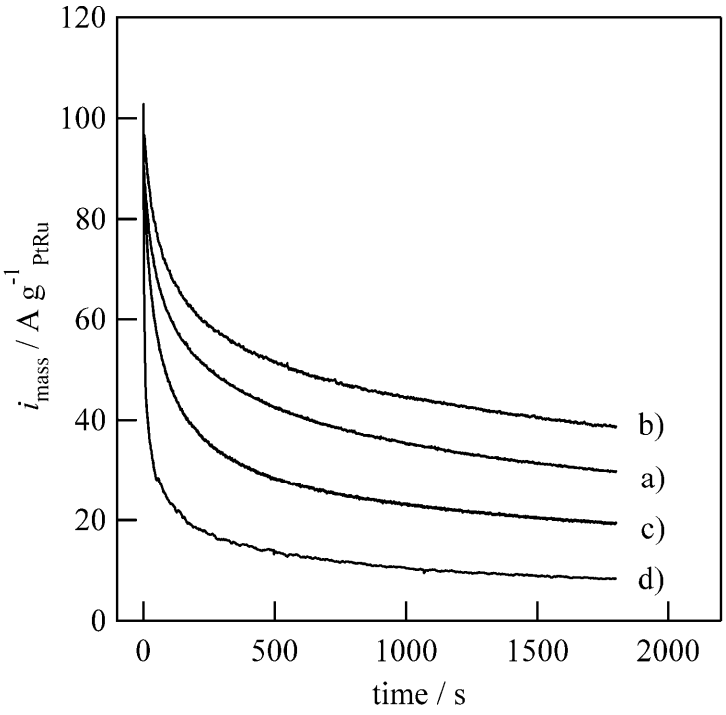
120
100
80
60
40
20
0
0
500
1000
1500
2000
time / s
i_{mass} / A g^{-1}_{PtRu}
b)
a)
c)
d)

Figure 14